Insertion of Vanadium(IV) Ions into the Polyoxotungstate Archetype

$\{As_4W_{40}\}$

Maria Stuckart,^{a,b} Natalya V. Izarova,^{a,b} Maria Glöβ,^{b,c} Jennifer Klose,^d Carolin Schmitz-Antoniak,^b Paul Kögerler,^{a,b} Berthold Kersting,^d Kirill Yu. Monakhov*,^c

^a Institute of Inorganic Chemistry, RWTH Aachen University, Landoltweg 1, 52074 Aachen,

Germany

^b Peter Grünberg Institute (PGI-6/7), JARA-FIT, Forschungszentrum Jülich GmbH, Wilhelm-Johnen-Straße, 52425 Jülich, Germany

 c Leibniz Institute of Surface Engineering (IOM), Permoserstraße 15, 04318 Leipzig, Germany

^d Institute of Inorganic Chemistry, Leipzig University, Johannisallee 29, 04103 Leipzig,

Germany

ABSTRACT

A new multi-metallic polyoxometalate wheel-shaped compound consisting of the 39-tungsto-4arsenate(III) unit (As4W39) with four incorporated V^{IV} ions (As4W39(V4)), isolated as $(NH_4)_{22}[(V^{IV}O)_2(V^{IV}O(H_2O))(As^{III}W^{VI}_9O_{33})_2(As^{III}W^{VI}_{8.5}V^{IV}_{0.5}(OH)O_{32})_2(WO_2)_4]\cdot 48H_2O \quad (\textbf{NH_4-})_{12}[(V^{IV}O)_2(V^{IV}O(H_2O))(As^{III}W^{VI}_9O_{33})_2(As^{III}W^{VI}_{8.5}V^{IV}_{0.5}(OH)O_{32})_2(WO_2)_4]\cdot 48H_2O \quad (\textbf{NH_4-})_{12}[(V^{IV}O)_2(V^{IV}O(H_2O))(As^{III}W^{VI}_9O_{33})_2(As^{III}W^{VI}_{8.5}V^{IV}_{0.5}(OH)O_{32})_2(WO_2)_4]\cdot 48H_2O \quad (\textbf{NH_4-})_{13}[(V^{IV}O)_2(V^{IV}O(H_2O))(As^{III}W^{VI}_9O_{33})_2(As^{III}W^{VI}_{8.5}V^{IV}_{0.5}(OH)O_{32})_2(WO_2)_4]\cdot 48H_2O \quad (\textbf{NH_4-})_{13}[(V^{IV}O)_2(V^{IV}O(H_2O))(As^{III}W^{VI}_9O_{33})_2(As^{III}W^{VI}_{8.5}V^{IV}_{0.5}(OH)O_{32})_2(WO_2)_4]\cdot 48H_2O \quad (\textbf{NH_4-})_{13}[(V^{IV}O)_2(V^{IV}O(H_2O))(As^{III}W^{VI}_9O_{33})_2(As^{III}W$ As4W₃₉(V₄)), was synthesized and fully characterized by spectroscopic, diffraction, thermogravimetric, electrochemical and magnetochemical methods. SQUID magnetometry showed three weakly coupled V^{IV} centers with an antiferromagnetic exchange interaction and one isolated V^{IV} as a spin-1/2 Curie paramagnet. The ultraviolet-visible spectroscopy measurements indicate the As4W39(V4) structure to remain intact in aqueous solution for at least 24 hours. To enable convenient deposition of As4W39(V4) from solution on gold surfaces under ultra-high vacuum, its tri(hexyl)(tetradecyl)phosphonium salt, THTDP-As4W39(V4), was prepared. The infrared spectra of both compounds revealed the structural identity of the As4W39(V4) polyanion independent of the countercations. The X-ray absorption near-edge structure spectroscopy confirmed the presence of V^{IV} centers in a distorted square pyramidal coordination geometry in NH4-As4W39(V4) and THTDP-As4W39(V4). The X-ray photoelectron spectra of the latter, deposited on an Au(111) surface, showed that the 4 vanadium and 35 tungsten centers preserve their +IV and +VI oxidation states, while the remaining 4 tungsten ions are reduced to +IV. This indicates that the As4W₃₉ wheel-like structure may serve as an insulating barrier for the controlled modification of electronic states of incorporated vanadium ions.

INTRODUCTION

The incorporation of vanadium ions in the wheel-like structure of polyoxometalates (POMs)¹⁻⁴ provides interesting opportunities^{5,6} to use V(3d) states for controlled electron transport and multiple-state resistive (memristive) switching.^{7,8} The wheel-shaped POM framework is envisaged here to prevent the hybridization of vanadium-centered molecular orbitals with electrode metal surfaces. In reduced POMs⁹ containing vanadium,¹⁰ vanadyl (VO²⁺) groups act as electron spin carriers, allowing for cooperative "molecular charge – redox – spin state" effects.

One of the promising POM candidates for these surface-oriented $^{11-17}$ studies is the 40-tungsto-4-arsenate(III) polyoxoanion [As4W40O140] $^{28-}$ (As4W40). It was shown that this inorganic cryptand can incorporate various transition metal ions, *e. g.* Ag1, 18 Co^{II}, 19 La^{III}, 20 Ce^{III}, 21 Pd^{II}, 22 in its inner cavity and furthermore can integrate V^{IV} or a mixture of V^{IV} and V^V ions. For instance, (NH4)20[{(V^{IV}O(H2O)(V^{IV}O)2)(NH4)2}{(As^{III}W9O33)4(WO2)4}] \cdot 40H2O and (NH4)23[{(K)(V^{IV}O)2}{(As^{III}W9O33)4(WO2)4}] \cdot nH2O contain exclusively V^{IV} ions in the inner cavity of the As4W40. These rare examples of As4W40 functionalization with vanadium(IV) ions lack, however, details on the crystal structure of these species. Another compound Na(NH4)20[{(V^{IV}O(H2O))(V^{IV}O)2(SO4)2}{(As^{III}W9O33)2(As^{III}W7.5V^V1.5O31)2(WO2)4}] \cdot 40H2O exemplifies the simultaneous replacement of three W^{VI} of As4W40 by V^V ions and the attachment of three V^{IV} ions to the resulting moiety. I

Here we describe the facile synthesis and characterization of a new derivative $(NH_4)_{22}[(V^{IV}O)_2(V^{IV}O(H_2O))(As^{III}W^{VI}_9O_{33})_2(As^{III}W^{VI}_{8.5}V^{IV}_{0.5}(OH)O_{32})_2(WO_2)_4]\cdot 48H_2O$ (hereafter referred to as **NH**₄-**As**₄**W**₃₉(**V**₄)) and report on its molecular solid-state structure determined by single-crystal X-ray diffraction accompanied by the analysis of molecular magnetic properties. The important insights into the adsorption characteristics of the polyanion

 $[(V^{IV}O)_2(V^{IV}O(H_2O))(As^{III}W^{VI}_9O_{33})_2(As^{III}W^{VI}_{8.5}V^{IV}_{0.5}(OH)O_{32})_2(WO_2)_4]^{22-} \quad \textbf{(As4W39(V4))} \quad \text{on solid substrates have been gained by X-ray photoelectron spectroscopy (XPS) for the $As4W39(V4)$ structure with tri(hexyl)(tetradecyl)phosphonium counterions (THTDP, <math display="block"> [CH_3(CH_2)_5]_3P^V(CH_2)_{13}CH_3\}^+) \text{ on the } Au(111) \text{ surface}.$

RESULTS AND DISCUSSION

The reaction of the pre-synthesized Na₂₇[NaAs₄W₄₀O₁₄₀]·60H₂O (Na-As₄W₄₀)²³ with VOSO₄·5H₂O in water (ratio of the components = 1:10) resulted in the formation of NH₄-As4W39(V4). The could latter also be obtained when pre-synthesized $[NH_4]_{23}[NH_4As_4W_{40}O_{140}(Co(H_2O))_2]\cdot 19H_2O(Co_2As_4W_{40})^{23}$ was used instead of Na-As₄W₄₀ (see Scheme 1 and the Supporting Information (SI) for details). Notably, the ratio of the components equal to 1:2 led to the functionalization of the As4W40 cavity with just two vanadium(IV) ions, affording the compound $(NH_4)_{24}[(V^{IV}O)_2(As^{III}W^{VI}_9O_{33})_4(WO_2)_4]\cdot 35H_2O$ $(NH_4-As_4W_{40}(V_2), see$ SI for details).

$$[NaAs_{4}W_{40}O_{140}]^{27-} \longrightarrow NH_{4}-As_{4}W_{39}(V_{4}) + [WO_{4}]^{2-} + Na^{+} \qquad (I)$$

$$[NH_{4}As_{4}W_{40}O_{140}(Co(H_{2}O))_{2}]^{23-} \longrightarrow NH_{4}-As_{4}W_{39}(V_{4}) + [WO_{4}]^{2-} + 2Co^{2+} \qquad (2)$$

Scheme 1. Reactions resulting in the formation of NH₄-As₄W₃₉(V₄).

The obtained compound NH₄-As₄W₃₉(V₄) was characterized in the solid state by FT-IR spectroscopy. The FT-IR spectrum of NH₄-As₄W₃₉(V₄) revealed some significant differences in comparison to that of the parent Na-As₄W₄₀ compound (Figure S1 and Table S1). The bands at 3135, 3019, 2802, and 1403 cm⁻¹ correspond to N-H vibrations of NH₄⁺ ions, which are present in

NH₄-**As**₄W₃₉(**V**₄). The band at around 835 cm⁻¹ is assigned to the W-O-V vibrations, which are absent in the spectrum of **Na**-**As**₄W₄₀. The broad band at around 1620 cm⁻¹, which belongs to asymmetric vibrations of crystal water molecules, and the band at *ca*. 890 cm⁻¹, which corresponds to As–O stretching modes, are observed in the both spectra.²⁴ The bands in the range 952 - 1012 cm⁻¹ in the spectra of **NH**₄-**As**₄W₃₉(**V**₄) and **NH**₄-**As**₄W₄₀(**V**₂) (see Table S1 in SI) can be assigned to the W=O and V=O vibrations.

The thermal stability of NH₄-As₄W₃₉(V₄) was investigated for a crystalline sample by thermogravimetric analysis (TGA) under nitrogen atmosphere. According to the TGA curve (Figure S4), the initial weight loss steps occur between 25 and 200 °C and correspond to the removal of 45 water molecules per formula unit (7.2 % found vs. 7.2 % calcd.). The number of water molecules determined by TGA is slightly lower than that obtained by elemental analysis (48 molecules). This can be explained by partial loss of crystal waters during sample drying and by higher degree of dryness for the sample used for TGA, which is a typical problem in POM chemistry as the relatively large number of water molecules is located in large voids between polyanions in the crystals and can be easily removed just in air or at slight heating. The further weight loss steps occurring in the range of 200 – 600 °C are attributed to the decomposition of NH₄-As₄W₃₉(V₄) and the release of 22 ammonia and 13 water molecules (5.0 % found vs. 5.4 % calcd.).

The electrochemical behavior of **NH**₄-**As**₄**W**₃₉(**V**₄) was studied in 1 M NH₄Cl solution by cyclic voltammetry. The stability of the **As**₄**W**₃₉(**V**₄) polyanions in this medium at least for 24 hours was confirmed using UV-vis spectroscopy (Figure S7). The CV curve of **NH**₄-**As**₄**W**₃₉(**V**₄) (Figure 1) exhibits a set of waves corresponding to sequential redox processes of W and V centers. The cathodic (at -0.58, -0.70 and -0.96 V) and anodic (at -0.35, -0.60 and -0.84 V) peak potentials

most probably represent the reduction and corresponding re-oxidation of the tungsten centers $W^{VI} \leftrightarrow W^{V}$; however, the redox process associated with one or more V centers $(V^{IV} \leftrightarrow V^{III})$ may also take place. The oxidation peaks at 0.43 and 0.63 V and corresponding reduction peaks at 0.38 and 0.53 V are assigned to the vanadium-centered redox processes $(V^{IV} \leftrightarrow V^{V})$ and $V^{IV} \leftrightarrow V^{VIII}$.

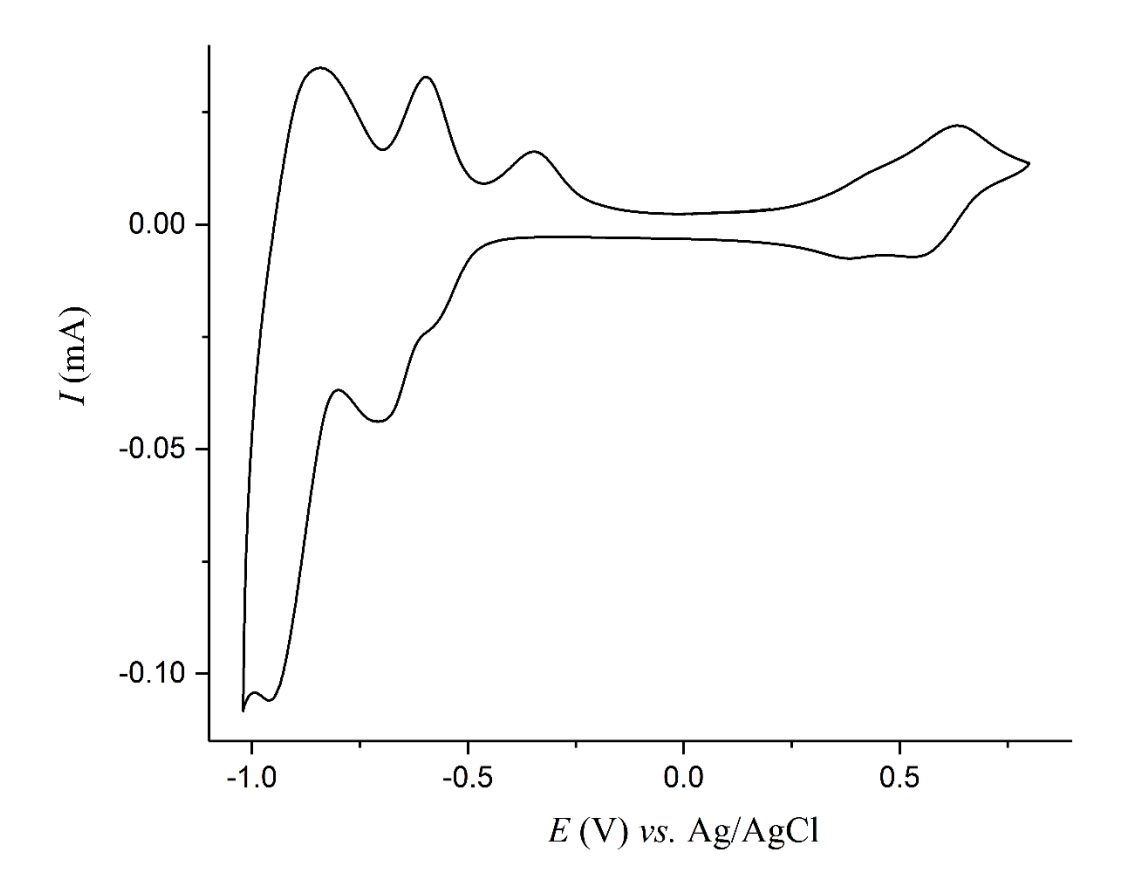


Figure 1. Cyclic voltammogram of 1 mM solution of **NH₄-As₄W₃₉(V₄)** in 1 M NH₄Cl *vs*. Ag/AgCl. Scan rate: 50 mV s⁻¹.

The molecular solid-state structure of the polyanion $As_4W_{39}(V_4)$ consists of the $\{As_4W_{39}V^{IV}O_{140}\}$ unit incorporating three V^{IV} ions in its inner cavity (Figure 2). The $\{As_4W_{39}V^{IV}O_{140}\}$ moiety is built up by three $\{AsW_9O_{33}\}$ units and one $\{AsW_8V^{IV}O_{33}\}$ unit, bridged by four $\{WO_6\}$ groups in

an alternating fashion. The $\{AsW_8V^{IV}O_{33}\}$ unit was formed by in situ metathesis of one W^{VI} center in the {AsW₉O₃₃} moiety by a V^{IV} ion. This V^{IV} ion is disordered with three W^{VI} centers in the two oppositely situated {AsW₈(W/V)O₃₃} groups of the polyanion (highlighted as dark green spheres in Figure 1). Bond valence sum (BVS) calculations^{26,27} revealed that one of the two terminal oxygens of two of these four {(W/V^{IV})O₆} groups interrelated by a mirror plane is monoprotonated (see gray spheres in Figure 2 and Table S3). The monoprotonated oxygens are directed toward the inner center of the wheel. One of the other three V^{IV} ions is octahedrally coordinated. It occupies the center of the {As₄W₃₉V^{IV}O₁₄₀} cavity and binds one oxygen atom from the every of four bridging {WO₆} groups (V–O 2.004(18)–2.063(15) Å). In addition, it coordinates terminal aqua (V–O 2.227(19) Å) and oxo (V–O 1.578(16) Å) ligands trans to each other (see Table S3 for the corresponding BVS values). At that, the agua ligand is directed toward the (W/V^{IV}) positions. Each of the remaining two "cavity" V^{IV} centers is coordinated by five oxygen atoms, forming a square pyramidal {V^{IV}O₅} unit. The {V^{IV}O₅} groups occupy opposite sites to each other and each of these V^{IV} ions coordinates two O atoms of the {AsW₉O₃₃} unit and one O atom from each neighboring {WO₆} group (V-O 1.909(15)-1.987(15) Å) as well as a terminal oxo ligand (V=O 1.617(16)–1.619(17) Å).

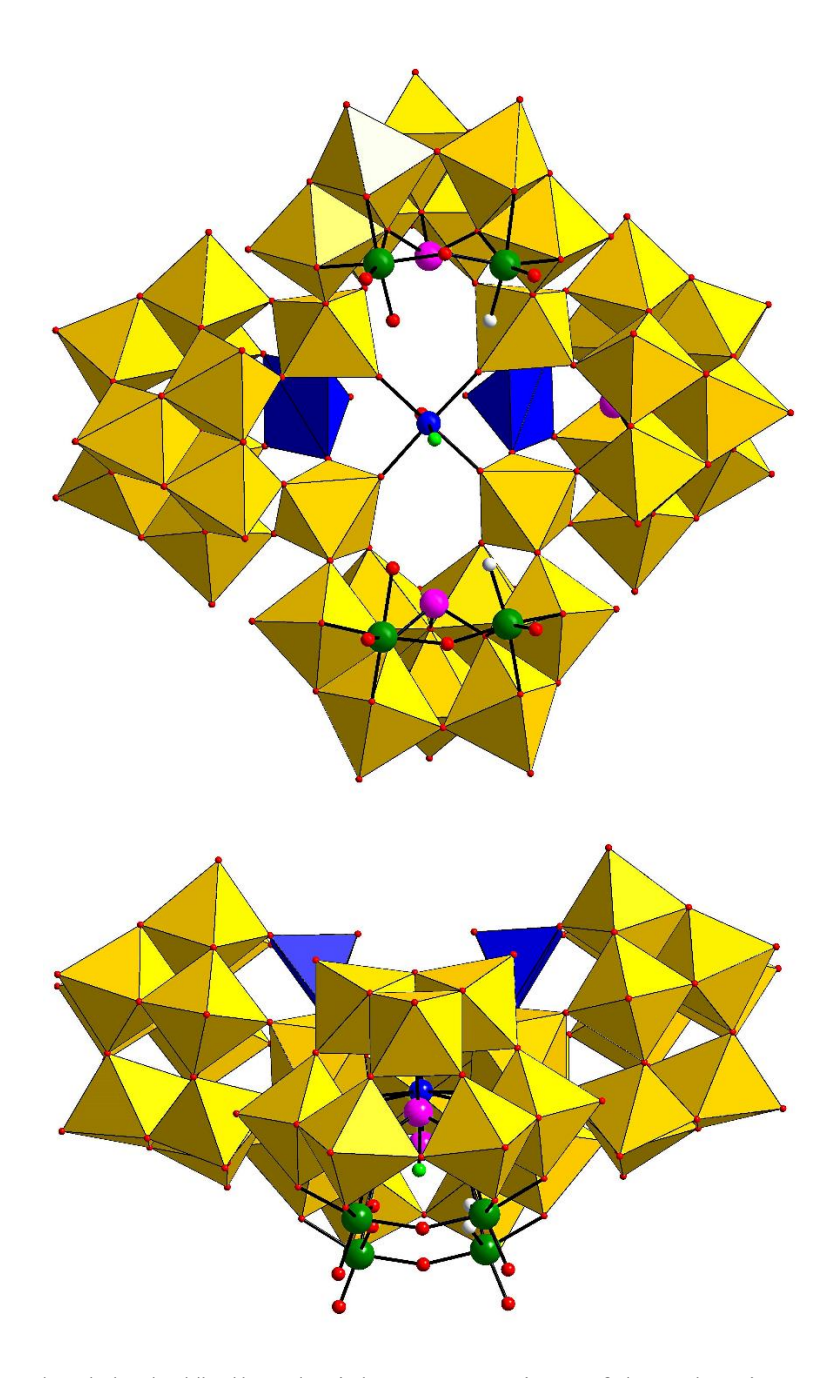


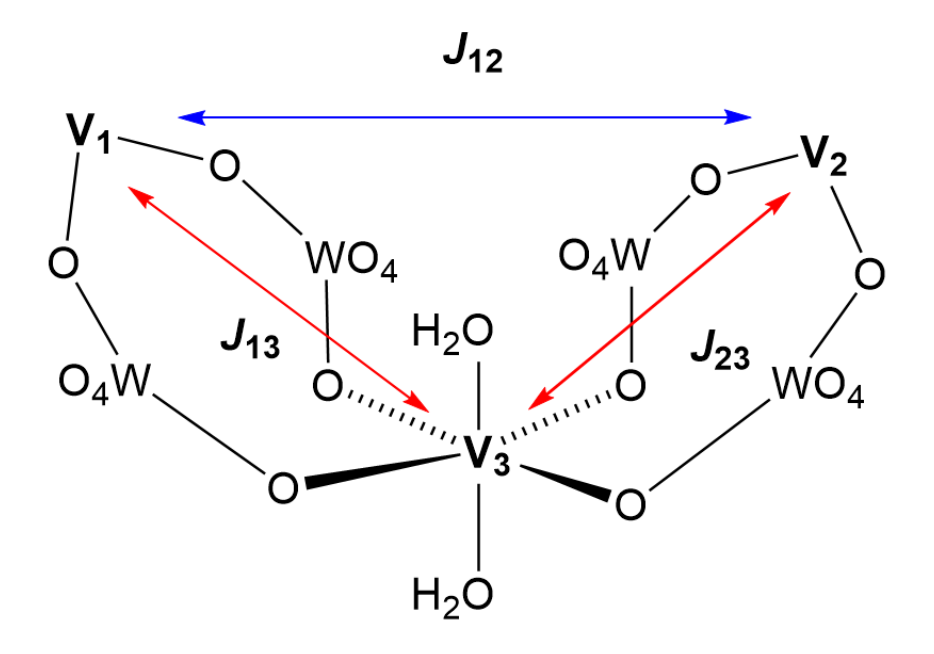
Figure 2. Combined polyhedral/ball-and-stick representations of the polyanion **As4W39(V4)** in two perpendicular views. Color legend: WO₆ yellow octahedra; {OVO₄} blue square pyramids; disordered V/W dark green, V blue, As pink, OH gray, H₂O bright green, O red spheres.

In the crystal lattice the $As_4W_{39}(V_4)$ polyanions form parallel rows along the crystallographic a axis (Figure S5). The polyanion units in one of the rows can be assumed to be arranged along the a axis, then, correspondingly, the polyanions in the neighboring rows are ordered in the opposite direction.

The magnetic characteristics of NH4-As4W39(V4) were studied by variable temperature dc magnetic susceptibility measurements using a SQUID-Magnetometer (MPMS Quantum Design). A powdered sample, desolvated at 80 °C in vacuum for prolonged time, was used for the measurements. Figure 3 displays a plot of the effective magnetic moment ($\mu_{\rm eff}$ per formula unit) versus T for NH₄-As₄W₃₉(V₄). At room temperature, $\mu_{\rm eff}$ amounts to 3.11 $\mu_{\rm B}$, which is slightly smaller than the theoretical value of 3.46 μ_B for four non-interacting vanadyl (VO²⁺) groups with an isotropic spin of s = 1/2 and a g factor very close to 2.²⁸ Upon decreasing temperature the μ_{eff} values decrease first slightly reaching 2.86 μ_B at 50 K and then more rapidly finally reaching 1.79 μ_B at 2 K, respectively. This decrease is most likely due to thermal depopulation of the V^{IV} ($S = \frac{1}{2}$) sublevels arising from spin-orbit coupling and the axial ligand field acting on the ${}^2T_{2g}$ ground term (in O_h symmetry). It has been shown that the ground term of V^{IV} complexes containing the vanadyl ion become effectively an orbital singlet as a result of the large axial crystal field such that a Curie law is obeyed giving $\mu_{\rm eff} = 1.73~\mu_{\rm B}$ independent of temperature. ^{29,30} However, our measurements show some temperature dependence of $\mu_{\rm eff}$ indicative of weak antiferromagnetic exchange interactions - as also seen for other polynuclear complexes containing oxovanadium(IV) centers.31-33

From a magnetochemical viewpoint, the **NH4-As4W39(V4)** compound contains three paramagnetic VO²⁺ units bridged by four diamagnetic W^{VI} centers and one isolated VO²⁺ unit (disordered over two sites). Despite a possible contribution of spin-orbit coupling and orbital degeneration of the

octahedrally coordinated central V^{IV} , we use the common Heisenberg-Dirac-van Vleck (HDvV) approximation to model the superexchange between the three paramagnetic VO^{2+} units.



Scheme 2. The exchange pattern between the V^{IV} ions in NH4-As4W39(V4).

The Heisenberg spin Hamiltonian for the trinuclear subunit is given by eq. 1. The two exchange parameters J and J' correspond to the exchange interactions between the adjacent and terminal V^{IV} centers, respectively, as sketched in Scheme 2.

$$\widehat{H} = -2J(\hat{S}_1\hat{S}_3 + \hat{S}_2\hat{S}_3) - 2J'(\hat{S}_1\hat{S}_2) \tag{1}$$

The magnetic susceptibility of the NH4-As4W39(V4) complex can be expressed by eq. 2, where χ_{trim} corresponds the susceptibility of the trinuclear subunit and χ_{mon} is the contribution of the isolated V^{IV} center.

$$\chi_{NH4As4W39(V4)} = \chi_{trim} + \chi_{mon} \tag{2}$$

To determine the magnitude of the exchange interactions J and J, the susceptibility data were analyzed by using the isotropic Heisenberg-Dirac-van Vleck (HDvV) exchange Hamiltonian

(eq. 1) for linear trinuclear V^{IV} complexes, which includes an additional temperature independent paramagnetism (TIP) term (which accounts for the contribution of the single V^{IV} ion treated as an isolated Curie ($S = \frac{1}{2}$ paramagnet) by using a full-matrix diagonalization approach.³⁴ Using this approach the experimental data could be satisfactorily fitted over the full temperature range, shown in Figure 3 as a red line. The parameters leading to the best fit were $J = -5.39 \text{ cm}^{-1}$, $J' = 0 \text{ cm}^{-1}$ (fixed), g = 2.02, and TIP = 0.00026 cm³ K mol⁻¹. Inclusion of the J' parameter did not improve the fit, and so it was fixed 0 cm⁻¹. These results are in reasonable agreement with broken symmetry density functional theory (DFT) calculations with the ORCA program package³⁵ yielding $J = -4.5 \text{ cm}^{-1}$. The antiferromagnetic coupling (J_{13}, J_{23}) between the terminal and central V^{IV} ions leads to a parallel spin alignment and a net ferromagnetic coupling J_{12} between the two terminal V^{IV} centers. More details about the DFT calculations can be found in SI. The superexchange interaction found in the present complex is significantly smaller than in μ -OH-bridged V^{IV} complexes.³⁶ This is attributed to the larger exchange coupling path through the WO₄²⁻ unit in NH4-As4W39(V4). Overall, the magnetic data for NH4-As4W39(V4) are in good agreement with the presence of four V^{IV} centers, three of which are weakly coupled in an antiferromagnetic exchange interaction, and one isolated V^{IV} site is acting as a S = 1/2 Curie paramagnet. At room temperature, the thermal energy is orders of magnitude larger than the exchange coupling (expressed in temperature units, J = -7.7 K), and thus explains the reasonable agreement of the measured effective magnetic moment (3.11 μ_B) with the theoretical value for four non-interacting V^{IV} ions $(3.46 \,\mu_{\rm B})$ mentioned above.

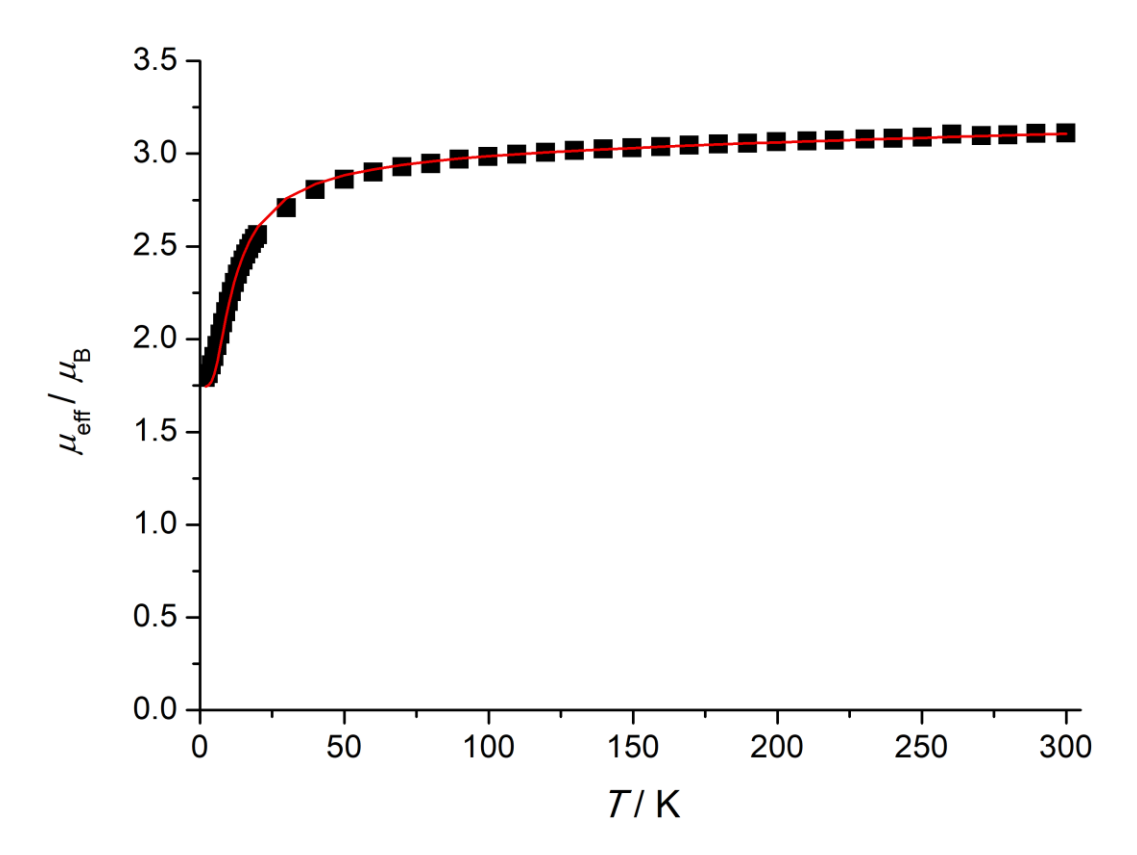


Figure 3. Plot of effective magnetic moment (μ_{eff}) vs temperature for NH₄-As₄W₃₉(V₄). The solid line is a fit of the data to the appropriate theoretical expression; see the text for the fitting parameters.

The structural and magnetic features of the heterometallic **As4W39(V4)** POM unit prompted us to gain insights into its stability on a solid support. Because the **NH4-As4W39(V4)** is insoluble in organic solvents, we isolated the title polyanion **As4W39(V4)** with {[CH3(CH2)5]3PV(CH2)13CH3}⁺ (**THTDP**) counterions using ion-exchange method³⁷ to allow for the deposition of the compound from cyclohexane on the metallic Au(111) surface, which eventually led to the formation of homogeneous layers. The structural identity of the POM unit of **THTDP-As4W39(V4)** as compared to that in **NH4-As4W39(V4)** was established based on the IR spectra of these compounds (see Figure S2 in SI).

In addition, the oxidation states of vanadium ions in both compounds were probed by X-ray absorption near-edge structure (XANES) spectroscopy. XANES spectra at the vanadium $L_{3,2}$ absorption edges of **NH4-As4W39(V4)** and **THTDP-As4W39(V4)** revealed clearly that the oxidation number of vanadium centers in both compounds is higher than +III. By comparison with theory, the main spectral features can be attributed to the presence of V^{IV} in a distorted square pyramidal coordination geometry (see SI for details).

To probe the electronic structure of **As₄W₃₉(V₄)** on a conducting metal surface, the **THTDP-As₄W₃₉(V₄)** compound was deposited on the Au(111) surface and assessed by X-ray photoelectron spectroscopy (XPS). The XPS spectrum of the **THTDP-As₄W₃₉(V₄)**/Au(111) sample (Figure 4) showed the 2p3/2 and 2p1/2 peaks in the V 2p core level region. The background was subtracted over the whole region of O 1s and V 2p. The fit resulted in two O 1s peaks and two V 2p peaks. For the O 1s peak we identified one peak as oxygen from metal oxides species at 530.4 eV and another O 1s peak at 532.1 eV was assigned to binding energies from organic impurities and hydroxides, respectively. At 523.1 eV we identified the V 2p1/2 peak and at 515.7 eV the V 2p3/2 peak. The fit gives no result for a second species of vanadium. The binding energy of the V 2p3/2 peak at 515.7 eV can be clearly assigned to a reduced vanadium state, likely in the plausible oxidation state +IV.

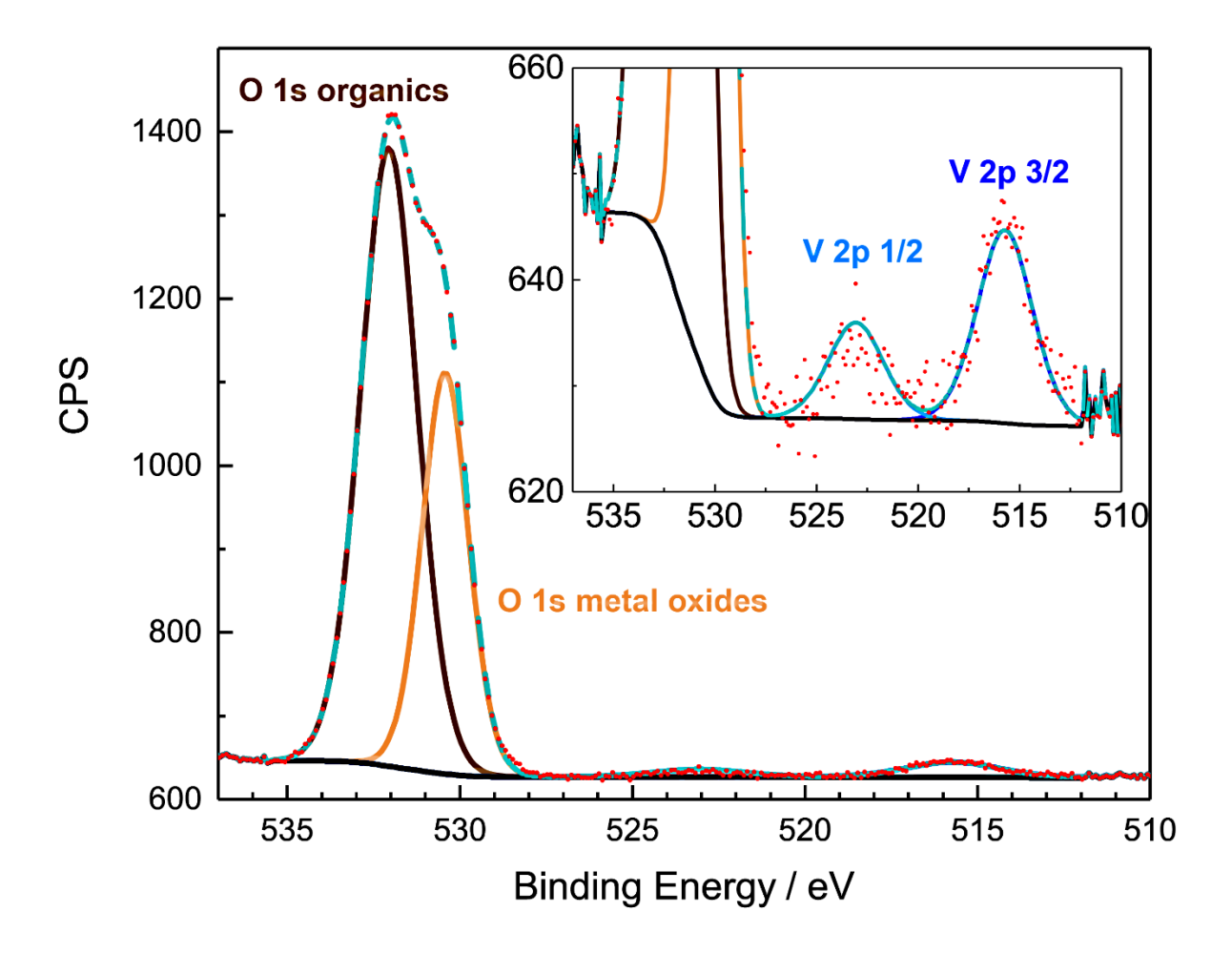


Figure 4. XPS core levels of oxygen 1s and vanadium 2p. Color code: red dots – experimental data, solid black line – background subtraction, cyan dashed line – envelope, solid blue line – fitted V 2p 3/2 core level, solid light blue line – fitted V 2p 1/2 core level, solid light brown line – fitted O 1s core level of metal oxides, solid brown line – fitted O 1s core level of organics and hydroxides.

The XPS spectrum of the W 4f core level region showed three peaks (Figure 5). The background was subtracted over the whole region. The fit resulted in six peaks (Figure 5). The peak at 35.5 eV is attributed to W 4f7/2 and the peak at 37.6 eV to W 4f5/2 of fully oxidized tungsten. There are two smaller peaks at 33.8 eV and 36.3 eV, respectively. These binding energies fit to the W 4f7/2

and W 4f5/2, respectively, of reduced tungsten in oxidation state +IV. The spectrum also contains two tungsten W 5p 3/2 signals at 41.3 eV and 39.0 eV, respectively. These binding energies are in good agreement with different measurements of fully oxidized tungsten containing POMs. ³⁸⁻⁴⁰ The area ratio of the two tungsten species is 90.9 % fully oxidized to 9.1 % reduced W. This thus corresponds to an atom ratio of 35 fully oxidized to 4 reduced tungsten atoms.

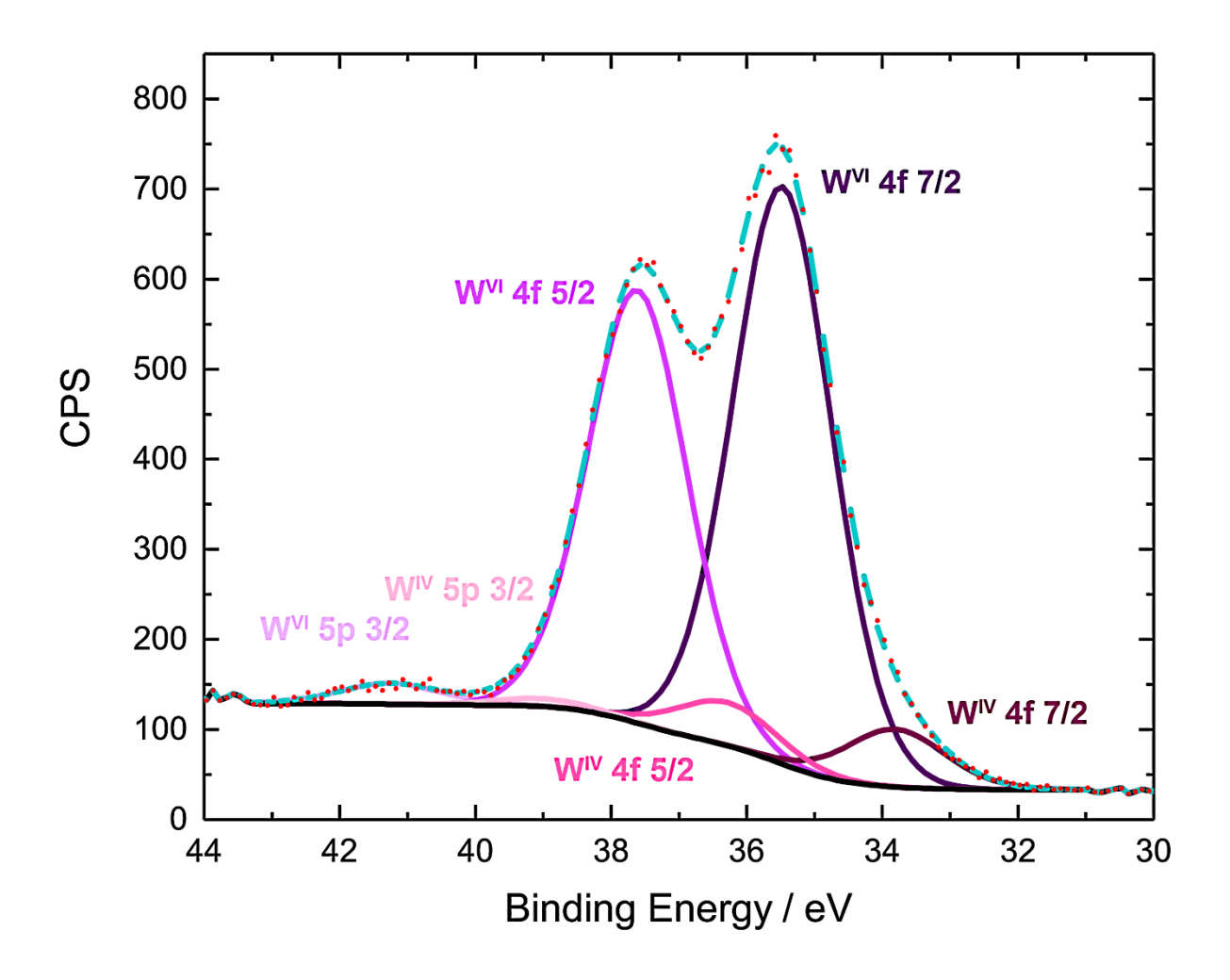


Figure 5. XPS 4f core level of tungsten. Color code: red dots – experimental data, solid black line – background subtraction, cyan dashed line – envelope, solid purple lines – fitted W^{VI} 4f and 5p core levels, solid pink lines – fitted W^{IV} 4f and 5 p core levels.

CONCLUSIONS

The V^{IV}-containing wheel-type POM compound NH₄-As₄W₃₉(V₄) was synthesized and fully

characterized. Its derivative THTDP-As4W39(V4), which is soluble in organic media, was

prepared to enable studies of this type of compound on gold surfaces under ultra-high vacuum. It

was shown that the As₄W₃₉(V₄) polyanion has appealing molecular properties in solution, ⁴¹ in the

solid state, and in contact with the metallic Au(111) surface. We currently study the **THTDP**-

As4W39(V4) compound and its other vanadium-containing derivatives on metallic and semi-

metallic substrates by high-resolution scanning probe microscopy and theoretical calculations.

Supporting Information. Details of synthesis, analytical characterization, magnetism. This

material is available free of charge via the Internet at http://pubs.acs.org.

Corresponding Author

* E-mail: kirill.monakhov@iom-leipzig.de. (K.Y.M.)

ORCID

Maria Stuckart: 0000-0002-2828-6309

Natalya Izarova: 0000-0001-5631-1930

Maria Glöß: 0000-0002-7914-0940

Carolin Schmitz-Antoniak: 0000-0002-8450-3515

Paul Kögerler: 0000-0001-7831-3953

16

Berthold Kersting: 0000-0001-5386-2809

Kirill Yu. Monakhov: 0000-0002-1013-0680

Notes

The authors declare no competing financial interests.

ACKNOWLEDGMENT

This work was supported by the Emmy Noether program of the Deutsche Forschungsgemeinschaft

(DFG). We thank Dr. Detlef Schmitz (Helmholtz-Zentrum Berlin) for scientific discussion and

providing the XANES data for V₂O₃. We are grateful to the Helmholtz-Zentrum Berlin (HZB) for

the allocation of synchrotron radiation beamtime.

REFERENCES

(1) Müller, A.; Pope, M. T.; Merca, A.; Bögge, H.; Schmidtmann, M.; Slageren, J.; Dressel,

M.; Kurth, D. G. A small cavity with reactive internal shell atoms spanned by four {As(W/V)₉}-

type building blocks allows host–guest chemistry under confined conditions. Chem. Eur. J. 2005,

11, 5849–5854.

(2) Müller, A.; Pope, M. T.; Todea A. M.; Bögge, H.; van Slageren, J.; Dressel, M.; Gouzerh,

P.; Thouvenot, R.; Tsukerblat, B.; Bell, A. Metal-oxide-based nucleation process under confined

conditions: two mixed-valence V₆-type aggregates closing the W₄₈ wheel-type cluster cavities.

Angew. Chem. Int. Ed. 2007, 46, 4477–4480.

17

- (3) Bassil, B. S.; Ibrahim, M.; Mal, S. S.; Suchopar, A.; Biboum, R. N.; Keita, B.; Nadjo, L.; Nellutla, S.; van Tol, J.; Dalal, N. S.; Kortz, U. Cobalt, manganese, nickel, and vanadium derivatives of the cyclic 48-tungsto-8-phosphate [H₇P₈W₄₈O₁₈₄]³³⁻. *Inorg. Chem.* **2010**, *49*, 4949–4959.
- (4) Assran, A. S.; Izarova, N. V.; Kortz, U. Mixed-valent vanadium substituted polyoxometalates: the wheel shaped $[Rb_{33}\{V^VV^{IV}_3O_7(H_2O)_6\}_2\{H_6P_6W_{39}O_{147}(H_2O)_3\}]^{15}$. CrystEngComm, **2010**, 12, 2684–2686.
- (5) Vilà-Nadal, L.; Mitchell, S. G.; Markov, S.; Busche, C.; Georgiev, V.; Asenov, A.; Cronin, L. Towards polyoxometalate-cluster-based nano-electronics. *Chem. Eur. J.* **2013**, *19*, 16502–16511.
- (6) Chen, X.; Zhou, Y.; Roy, V.A.L.; Han, S.T. Evolutionary metal oxide clusters for novel applications: toward high-density data storage in nonvolatile memories. *Adv. Mater.* **2018**, *30*, 1703950.
- (7) Linnenberg, O.; Moors, M.; Notario-Estévez, A.; López, X.; de Graaf, C.; Peter, S.; Bäumer, C.; Waser, R.; Monakhov, K. Y. Addressing multiple resistive states of polyoxovanadates: conductivity as a function of individual molecular redox states. *J. Am. Chem. Soc.* **2018**, *140*, 16635–16640.
- (8) Li, Y.; Qian, Q.; Zhu, X.; Li, Y.; Zhang, M.; Li, J.; Ma, C.; Li, H.; Lu, J.; Zhang, Q. Recent advances in organic-based materials for resistive memory applications. *InfoMat* **2020**, 2, 995–1033.
- (9) Gumerova, N.; Rompel, A. Synthesis, structures and applications of electron-rich polyoxometalates. *Nat. Rev. Chem.* **2018**, *2*, 0112.

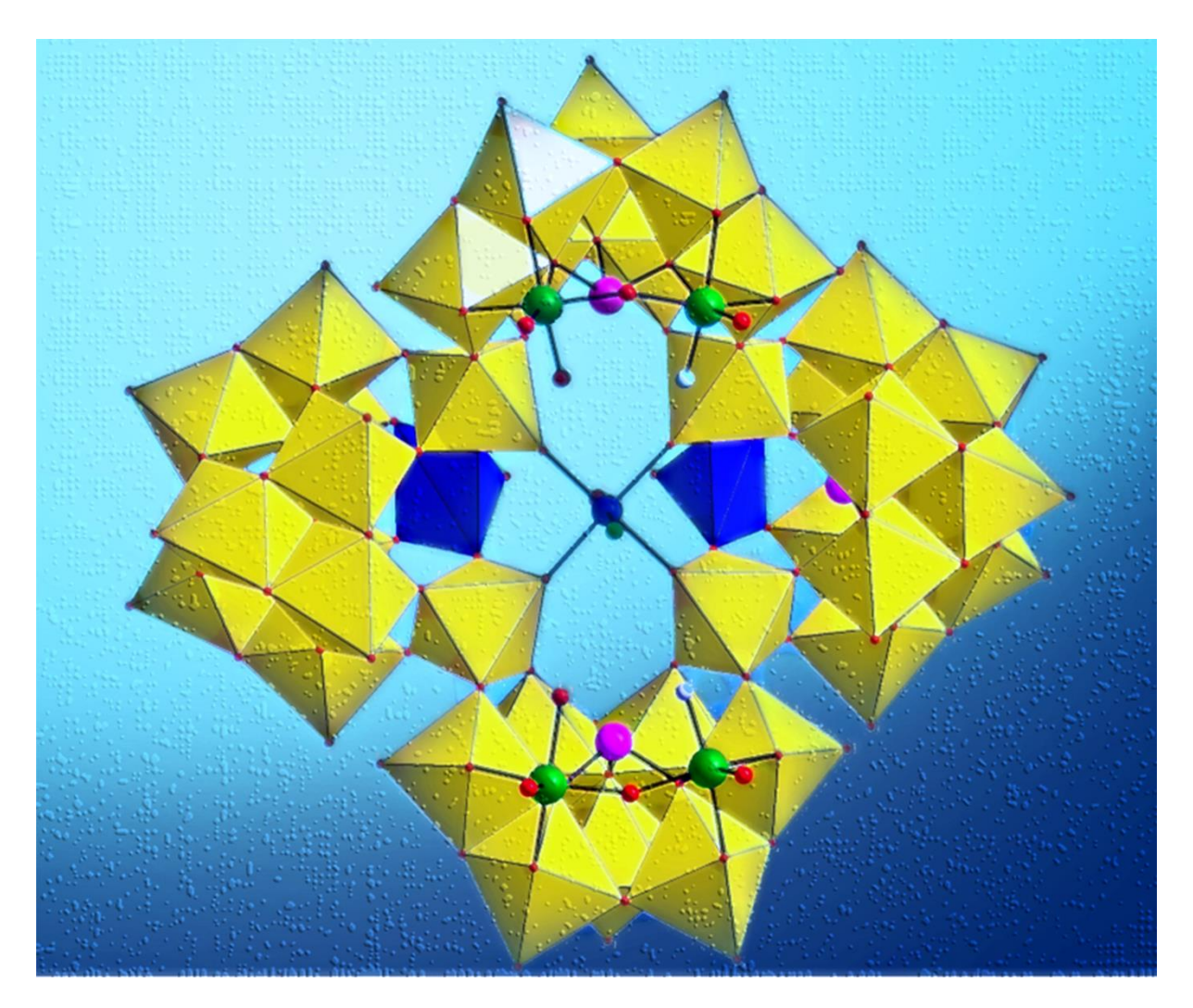
- (10) Stuckart, M.; Monakhov, K.Y. Vanadium: polyoxometalate chemistry. In *Encyclopedia of Inorganic and Bioinorganic Chemistry*; Scott, R.A., Ed.; John Wiley & Sons, Ltd.: Chichester, 2018; pp 1–19.
- (11) Alam, M. S.; Dremov, V.; Müller, P.; Postnikov, A. V.; Mal, S. S.; Hussain, F.; Ulrich Kortz, U. STM/STS observation of polyoxoanions on HOPG surfaces: the wheel-shaped $[Cu_{20}Cl(OH)_{24}(H_2O)_{12}(P_8W_{48}O_{184})]^{25}$ and the ball-shaped $[Sn(CH_3)_2(H_2O)]_{24}[Sn(CH_3)_2]_{12}(A-PW_9O_{34})_{12}]^{36}$. *Inorg. Chem.* **2006**, *45*, 2866–2872.
- (12) Volatron, F.; Noël, J.-M.; Rinfray, C.; Decorse, P.; Combellas, C.; Kanoufi, F.; Proust, A. Electron transfer properties of a monolayer of hybrid polyoxometalates on silicon. *J. Mater. Chem. C* **2015**, *3*, 6266–6275.
- (13) Lombana, A.; Rinfray, C.; Volatron, F.; Izzet, G.; Battaglini, N.; Alves, S.; Decorse, P.; Lang, P.; Proust, A. Surface organization of polyoxometalate hybrids steered by a 2D supramolecular PTCDI/melamine network. *J. Phys. Chem. C* **2016**, *120*, 2837–2845.
- (14) Yi, X.; Izarova, N. V.; Stuckart, M.; Guérin, D.; Thomas, L.; Lenfant, S.; Vuillaume, D.; van Leusen, J.; Duchoň, T.; Nemšák, S.; Bourone, S. D. M.; Schmitz, S.; Kögerler, P. Probing frontier orbital energies of {Co₉(P₂W₁₅)₃} polyoxometalate clusters at molecule–metal and molecule–water interfaces. *J. Am. Chem. Soc.* **2017**, *139*, 14501–14510.
- (15) Laurans, M.; Francesca, K.D.; Volatron, F.; Izzet, G.; Guerin, D.; Vuillaume, D.; Lenfant, S.; Proust, A. Molecular signature of polyoxometalates in electron transport of silicon-based molecular junctions. *Nanoscale* **2018**, *10*, 17156–17165.
- (16) Zhu, Q.; Paci, B.; Generosi, A.; Renaudineau, S.; Gouzerh, P.; Liang, X.; Mathieu, C.; Rountree, C.; Izzet, G.; Proust, A. Conductivity via thermally induced gap states in a polyoxometalate thin layer. *J. Phys. Chem. C* **2019**, *123*, 1922–1930.

- (17) Cherevan, A.S.; Nandan, S.P.; Roger, I.; Liu, R.; Streb, C.; Eder, D. Polyoxometalates on functional substrates: concepts, synergies, and future perspectives. *Adv. Sci.* **2020**, *7*, 1903511.
- (18) Leyrie, M.; Hervé, G. Synthesis and chemical behaviour of a new heteropolytungstate: $(M_nAs_4W_{40}O_{140})^{(28-n)}$, an inorganic cryptate $(M^{n+} = Na^+, K^+, Ba^{2+})$. *Nouv. J. Chim.* **1978**, 2, 233–237.
- (19) Robert, F.; Leyrie, M.; Hervé, G.; Tézé, A.; Jeannin, Y. Crystal structure of ammonium dicobalto(II)-40-tungstotetraarsenate(III). Allosteric effects in the ligand. *Inorg. Chem.* **1980**, *19*, 1746–1752.
- (20) Liu, J.; Guo, J.; Zhao, B.; Xu, G.; Li, M. Synthesis and characterization of novel heteropolytungstoarsenate containing lanthanum (LaAs₄W₄₀O₁₄₀)²⁵ and its derivatives (LaAs₄W₄₀O₁₄₀M₂)ⁿ. *Transition Met. Chem.* **1993**, *18*, 205–208.
- (21) Wassermann, K.; Pope, M. T. Large cluster formation through multiple substitution with lanthanide cations (La, Ce, Nd, Sm, Eu, and Gd) of the polyoxoanion [(B-α-AsO₃W₉O₃₀)₄(WO₂)₄]²⁸⁻. Synthesis and structural characterization. *Inorg. Chem.* **2001**, *40*, 2763–2768.
- (22) Lin, Z.; Izarova, N. V.; Mehari, F. T.; Kortz, U. Palladium(II) incorporation in the all-inorganic cryptand $[As_4W_{40}O_{140}]^{28-}$: Synthesis and structural characterization of $[Pd_2Na_2KAs_4W_{40}O_{140}(H_2O)]^{21-}$. Z. Anorg. Allg. Chem. **2018**, 644, 1379–1382.
- (23) Hervé, G.; Tézé, A. Tetracontatungstotetraarsenate (III) and its cobalt(II) complex. In *Inorganic Synthesis*; Ginsberg, A.P., Ed.; Wiley, 1990, Vol. 27, pp 118–120.
- (24) Nakamoto, K. *Infrared and Raman spectra of inorganic and coordination compounds Part A: Theory and applications in inorganic chemistry*, 5th ed.; Wiley and Sons: New York, **1997**.

- (25) Galloni, P.; Conte, V.; Floris, B. A journey into the electrochemistry of vanadium compounds. *Coord. Chem. Rev.* **2015**, *301–302*, 240–299.
- (26) Brown, I. D.; Altermatt, D. Bond-valence parameters obtained from a systematic analysis of the inorganic crystal structure database. *Acta Crystallogr.*, *Sect. B* **1985**, *41*, 244–247.
- (27) Knížek, K. Kalvados Software for crystal structure and powder diffraction; see http://www.fzu.cz/~knizek/kalvados/index.html.
- (28) Karet, G. B.; Sun, Z.; D. D. Heinrich, D. D.; McCusker, J. K.; Folting, K.; Streib, W. E.; Huffman, J. C.; Hendrickson, D. N.; Christou, G. Tetranuclear and pentanuclear vanadium(IV/V) carboxylate complexes: $[V_4O_8(NO_3)(O_2CR)_4]^{2-}$ and $[V_5O_9X(O_2CR)_4]^{2-}$ ($X = Cl^-$, Br^-) salts. *Inorg. Chem.* **1996**, *35*, 6450–6460.
- (29) Figgis, B. N.; Lewis, J. *Progress in Inorganic Chemistry*; Interscience, 1964, Vol. 6, p. 37.
- (30) Ballhausen, C. J.; Gray, H. B. The electronic structure of the vanadyl ion. *Inorg. Chem.* **1962**, *1*, 111–122.
- (31) Machin, D. J.; Murray, K. S. The magnetic properties of some vanadium(IV) complexes. *J. Chem. Soc. A* **1967**, 1330–1332.
- (32) Toftlund, H.; Larsen, S.; Murray, K. S. Synthesis and spectroscopic and magnetic properties of a unique diamagnetic binuclear μ -oxo vanadium(IV) complex. Crystal structure of [(tpa)VO(μ -O)VO(tpa)](ClO₄)₂ (tpa = tris(2-pyridylmethyl)amine). *Inorg. Chem.* **1991**, *30*, 3964–3967.
- (33) Wieghardt, K.; Bossek, U.; Volckmar, K.; Swiridoff, W.; Weiss, J. Synthesis and crystal structure of bis(μ -hydroxo)bis[oxo(1,4,7-triazacyclononane)vanadium(IV)] dibromide, a μ -hydroxo-bridged cation with antiferromagnetically coupled V(IV) centers. *Inorg. Chem.* **1984**, *23*, 1387–1389.

- (34) Azuah, R. T.; Kneller, L. R.; Qiu, Y.; Tregenna-Piggott, P. L. W.; Brown, C. M.; Copley, J. R. D.; Dimeo, R. M. J. DAVE: a comprehensive software suite for the reduction, visualization, and analysis of low energy neutron spectroscopic data. *J. Res. Natl. Inst. Stand. Technol.* **2009**, *114*, 341–358.
- (35) Neese, F. The ORCA program system. *Wiley Interdiscip. Rev.* **2012**, 2, 73–78.
- (36) Bazhina, E. S.; Aleksandrov, G. G.; Kiskin, M. A.; Efimov, N. N.; Ugolkova, E. A.; Korlyukov, A. A.; Nikitin, O. M.; Magdesieva, T. V.; Minin, V. V.; Sidorov, A. A.; Miller, J. S.; Eremenko, I. L. Synthesis, crystal structure and spin exchange coupling in polynuclear carboxylates with {Li₂(VO)₂} metal core. *Polyhedron* **2017**, *137*, 246–255.
- (37) Misra, A.; Castillo, I. F.; Daniel P. Müller, D. P.; González, C.; Eyssautier-Chuine, S.; Ziegler, A.; de la Fuente, J. M.; Mitchell, S. G.; Streb, C. Polyoxometalate-ionic liquids (POM-ILs) as anticorrosion and antibacterial coatings for natural stones. *Angew. Chem. Int. Ed.* **2018**, *57*, 14926–14931.
- (38) Nagai, M.; Sanpei, H.; Shirakura, M. Cobalt porphyrin–tungsten polyoxometalate anion as non-noble metal cathode catalyst in a fuel cell. *J. Mater. Chem.* **2012**, 22, 9222–9229.
- (39) Ponja, S. D.; Sathasivam, S.; Davies, H. O.; Parkin, I. P.; Carmalt, C. J. Polyoxometalate complexes as precursors to vanadium-doped molybdenum or tungsten oxide thin films by means of aerosol-assisted chemical vapour deposition. *ChemPlusChem* **2016**, *81*, 307–314.
- (40) Glöß, M.; Pütt, R.; Moors, M.; Kentzinger, E.; Pyckhout-Hintzen, W.; Monakhov, K. Y. Interplaying the amphipathic polyoxometalate interactions in solution and at solid–liquid interfaces: A toolbox for the technical application. *Nanoscale* **2019**, *11*, 4267–4277.
- (41) Gumerova, N. I.; Rompel, A. Polyoxometalates in solution: speciation under spotlight. *Chem. Soc. Rev.* **2020**, *49*, 7568–7601.

TABLE OF CONTENTS GRAPHIC AND SYNOPSIS



The X-ray crystal structure shows a paramagnetic, redox-active wheel-shaped polyoxotungstate incorporating As^{III} and V^{IV} ions, which has the potential for controlled electron modification on surfaces.